On-Demand Degradation of Metal-Organic Framework based on Photocleavable Dianthracene-based Ligand

Guillaume Collet,[*,†] Timothée Lathion,[†] Céline Besnard,[‡] Claude Piguet,[†] Stéphane Petoud[*,†,§]

[†] Department of Inorganic and Analytical Chemistry, University of Geneva, 30 Quai E Ansermet, CH-1211 Geneva 4, Switzerland

[‡] Laboratory of Crystallography, University of Geneva, 30 Quai E Ansermet, CH-1211 Geneva 4, Switzerland

[§] Centre de Biophysique Moléculaire (CBM) ; UPR CNRS 4301, Rue Charles Sadron, F-45071 Orléans 2, France

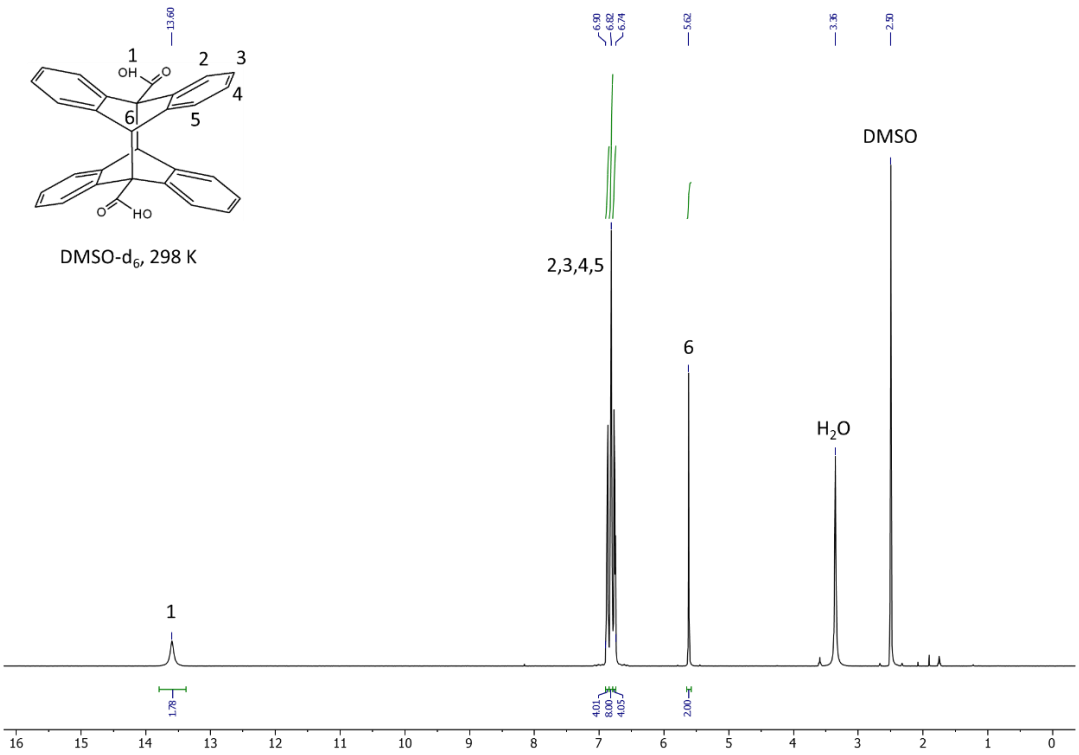

Figure S1: ^{1}H NMR spectrum of Di-9AC, DMSO-d_6, 298 K.

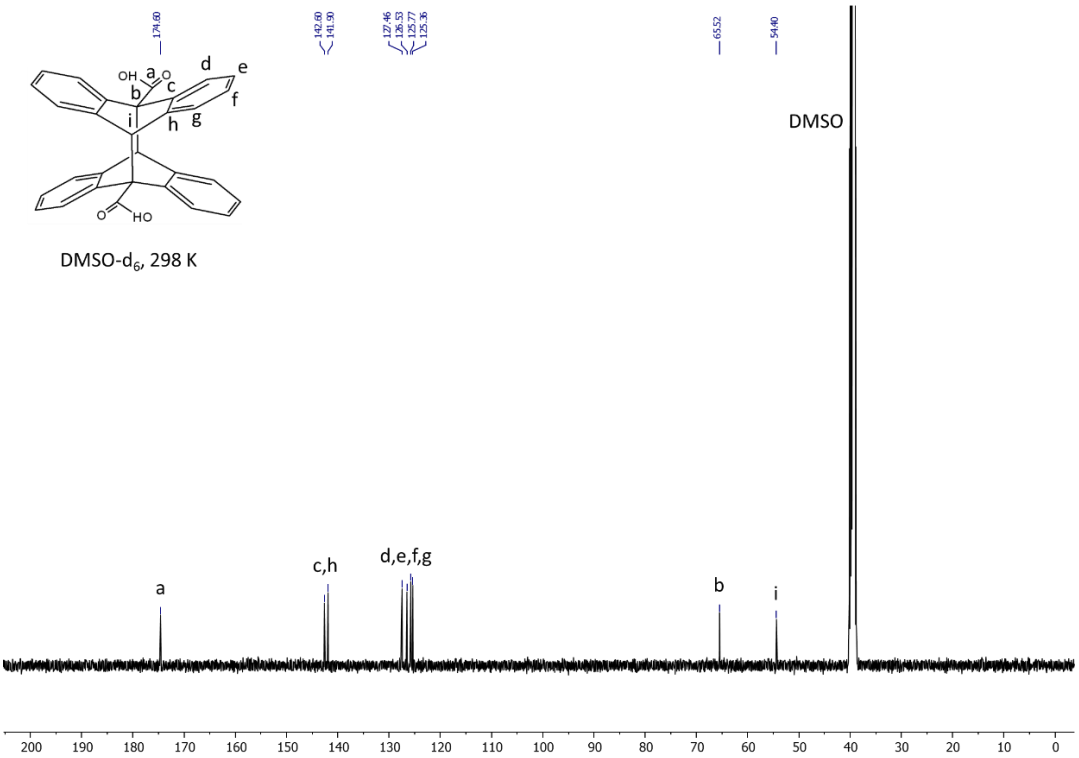

Figure S2: ^{13}C NMR spectrum of Di-9AC, DMSO-d_6, 298 K.

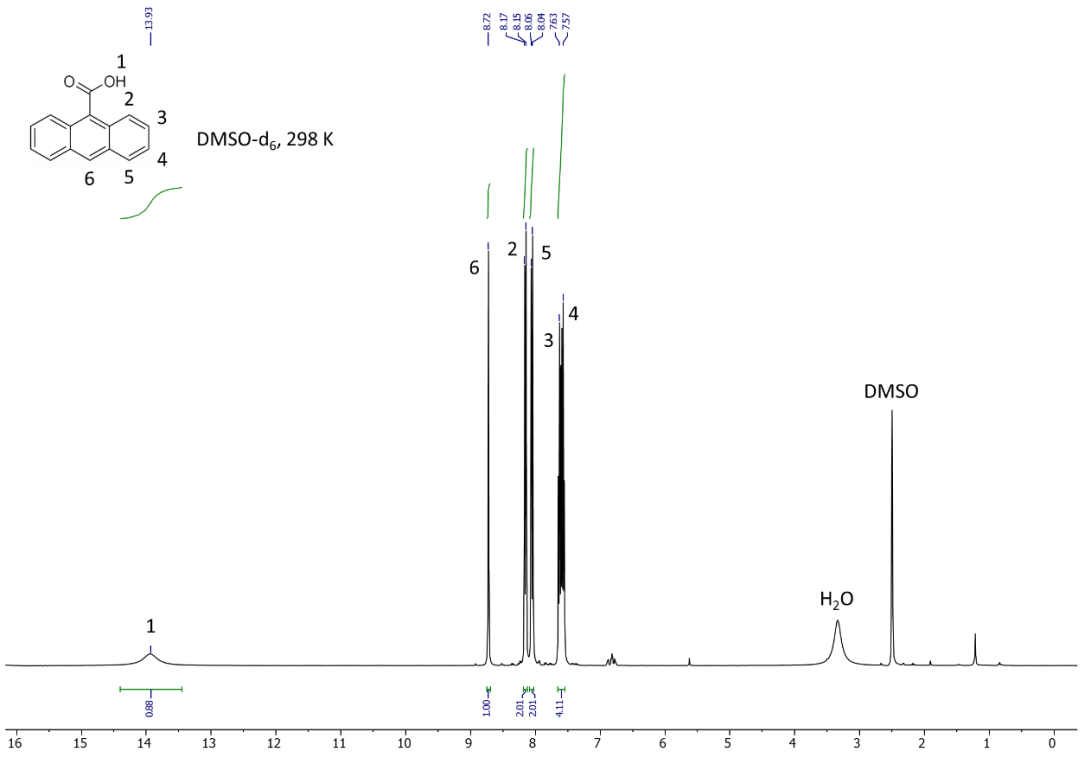

Figure S3: ^{1}H NMR spectrum of 9AC, DMSO-d_6, 298 K.

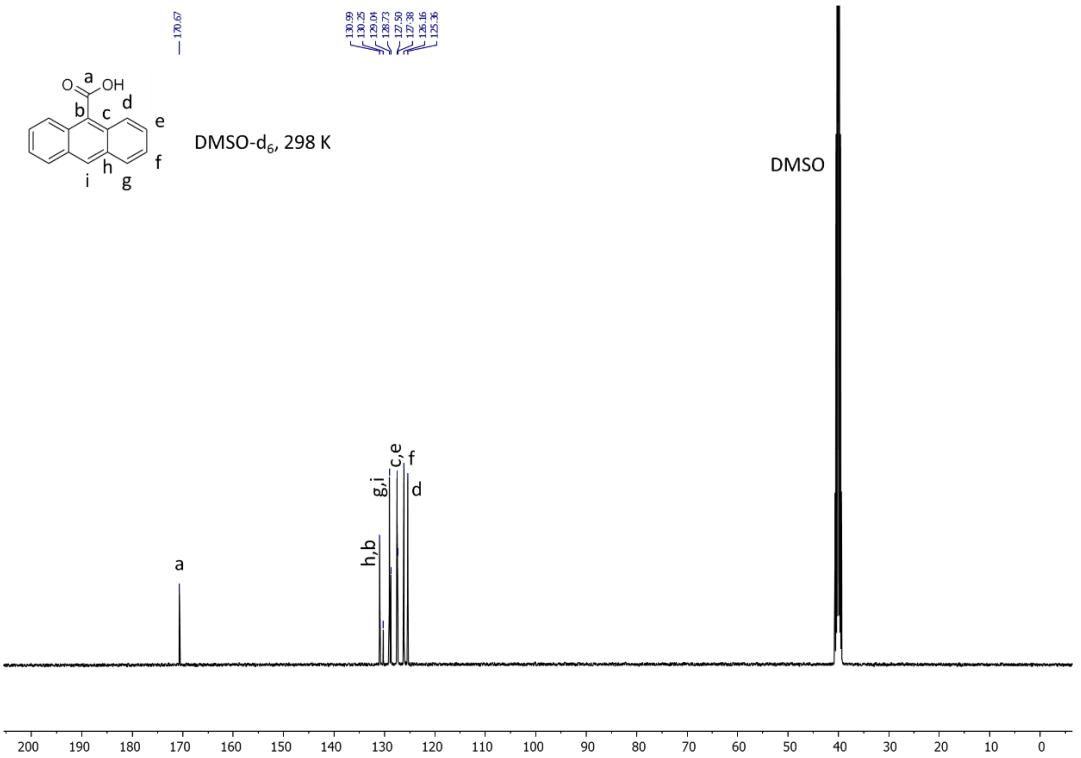

Figure S4: ^{13}C NMR spectrum of 9AC, DMSO-d_6, 298 K.

Table S1: Crystal data and structure refinement for Di-9AC crystallized in DMSO by slow evaporation

CCDC number	1835667
Empirical formula	$C_{34}H_{32}O_6S_2$
Formula weight	600.71
Temperature/K	180.00(10)
Crystal system	monoclinic
Space group	$P2_1/n$
a/Å	10.4209(3)
b/Å	7.9301(2)
c/Å	18.7758(5)
α/°	90
β/°	104.060(3)
γ/°	90
Volume/Å^3	1505.13(7)
Z	2
ρ_{calc}g/cm^3	1.325
μ/mm^{-1}	1.972
F(000)	632.0
Crystal size/mm^3	0.634 × 0.513 × 0.302
Radiation	CuKα (λ = 1.54184)
2Θ range for data collection/°	8.914 to 146.678
Index ranges	$-12 \leq h \leq 12$, $-9 \leq k \leq 5$, $-23 \leq l \leq 22$
Reflections collected	4930
Independent reflections	2934 [R_{int} = 0.0177, R_{sigma} = 0.0201]
Data/restraints/parameters	2934/0/196
Goodness-of-fit on F^2	1.044
Final R indexes [I>=2σ (I)]	R_1 = 0.0486, wR_2 = 0.1298
Final R indexes [all data]	R_1 = 0.0500, wR_2 = 0.1311
Largest diff. peak/hole / e Å^{-3}	0.53/-0.54

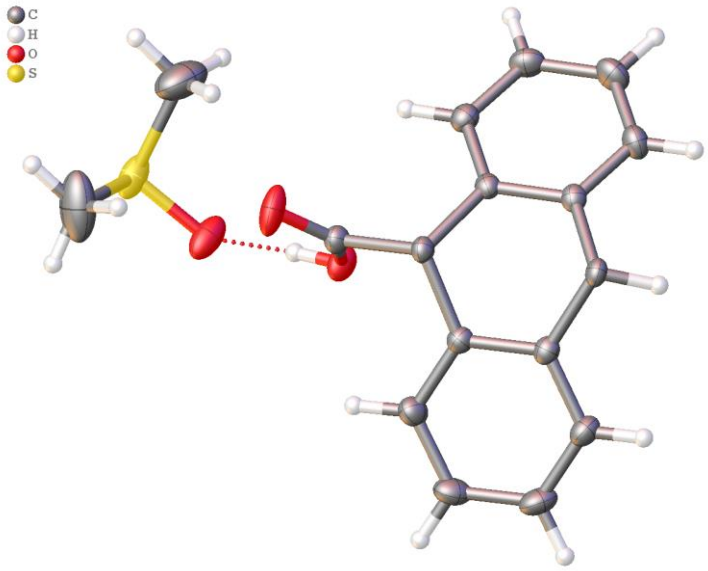

Figure S5: View of the asymmetric unit. Displacement ellipsoids are depicted at 50 percent probability level for Di-9AC crystallized in DMSO by slow evaporation.

Table S2: Crystal data and structure refinement for Di-9AC crystallized in DMA by warming up to 130°C and then cooling down to room temperature.

CCDC number	1835666
Empirical formula	$C_{38}H_{38}N_2O_6$
Formula weight	618.70
Temperature/K	180.01(10)
Crystal system	monoclinic
Space group	$P2_1/c$
a/Å	10.6198(3)
b/Å	12.0108(3)
c/Å	12.5761(3)
α/°	90
β/°	96.716(2)
γ/°	90
Volume/Å^3	1593.10(7)
Z	2
ρ_{calc}g/cm^3	1.290
μ/mm^{-1}	0.704
F(000)	656.0
Crystal size/mm^3	0.114 × 0.06 × 0.039
Radiation	CuKα (λ = 1.54184)
2Θ range for data collection/°	8.384 to 147.126
Index ranges	$-13 \leq h \leq 11$, $-14 \leq k \leq 14$, $-9 \leq l \leq 15$
Reflections collected	5834
Independent reflections	3122 [R_{int} = 0.0226, R_{sigma} = 0.0339]
Data/restraints/parameters	3122/0/214
Goodness-of-fit on F^2	1.043
Final R indexes [I>=2σ (I)]	R_1 = 0.0404, wR_2 = 0.1004
Final R indexes [all data]	R_1 = 0.0507, wR_2 = 0.1082
Largest diff. peak/hole / e Å^{-3}	0.27/-0.25

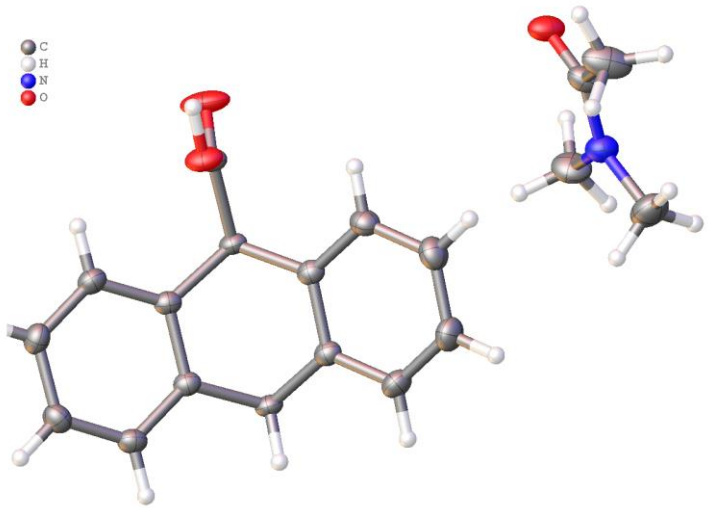

Figure S6: View of the asymmetric unit. Displacement ellipsoids are depicted at 50 percent probability level for Di-9AC crystallized in DMA by warming up to 130°C and then cooling down to room temperature.

Table S3: Crystal data and structure refinement for Di-9AC crystallized in DMA by slow evaporation.

CCDC number	1835665
Empirical formula	$C_{38}H_{38}N_2O_6$
Formula weight	618.70
Temperature/K	180.00(10)
Crystal system	triclinic
Space group	P-1
a/Å	9.2901(5)
b/Å	13.6758(7)
c/Å	14.4243(8)
α/°	66.913(5)
β/°	74.315(5)
γ/°	74.609(4)
Volume/Å^3	1596.55(16)
Z	2
ρ_{calc}g/cm^3	1.287
μ/mm^{-1}	0.703
F(000)	656.0
Crystal size/mm^3	0.174 × 0.162 × 0.02
Radiation	CuKα (λ = 1.54184)
2Θ range for data collection/°	6.782 to 147.568
Index ranges	$-11 \leq h \leq 11$, $-16 \leq k \leq 16$, $-14 \leq l \leq 17$
Reflections collected	10783
Independent reflections	6235 [R_{int} = 0.0259, R_{sigma} = 0.0372]
Data/restraints/parameters	6235/2/428
Goodness-of-fit on F^2	1.017
Final R indexes [I>=2σ (I)]	R_1 = 0.0418, wR_2 = 0.1030
Final R indexes [all data]	R_1 = 0.0548, wR_2 = 0.1132
Largest diff. peak/hole / e Å^{-3}	0.52/-0.29

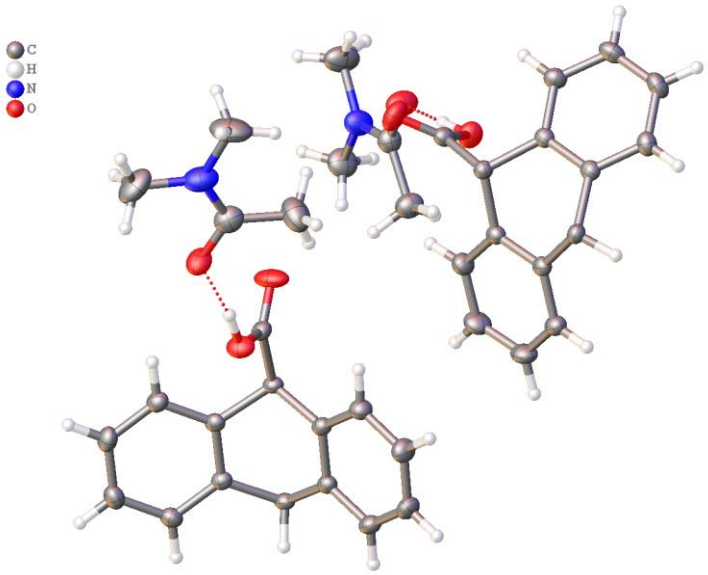

Figure S7: View of the asymmetric unit. Displacement ellipsoids are depicted at 50 percent probability level for Di-9AC crystallized in DMA by slow evaporation.

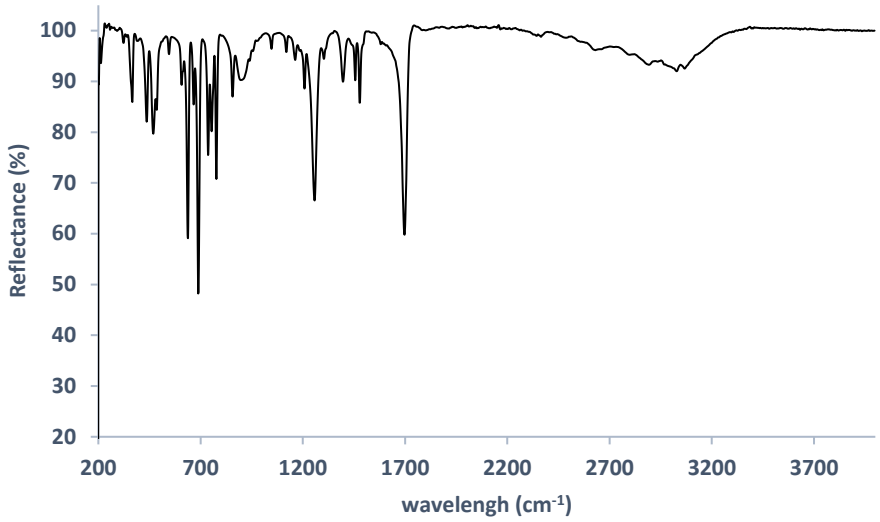

Figure S8: FTIR spectrum of Di-9AC.

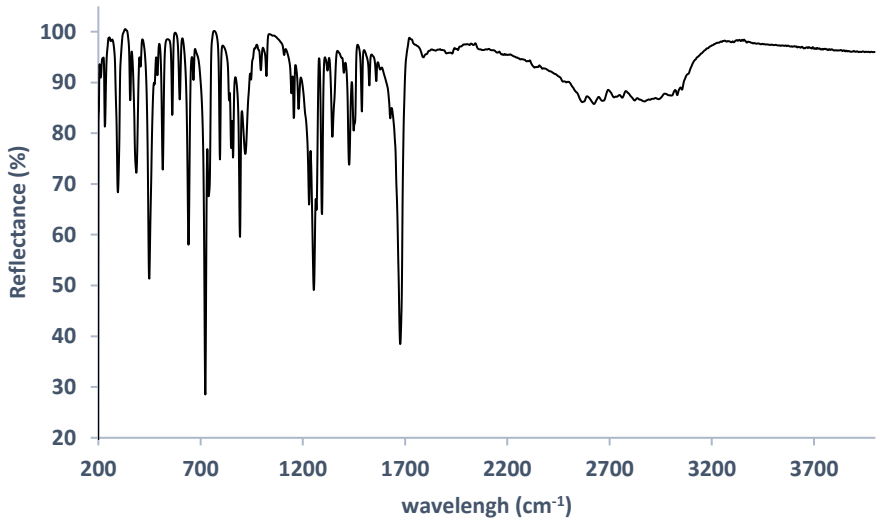

Figure S9: FTIR spectrum of 9AC.

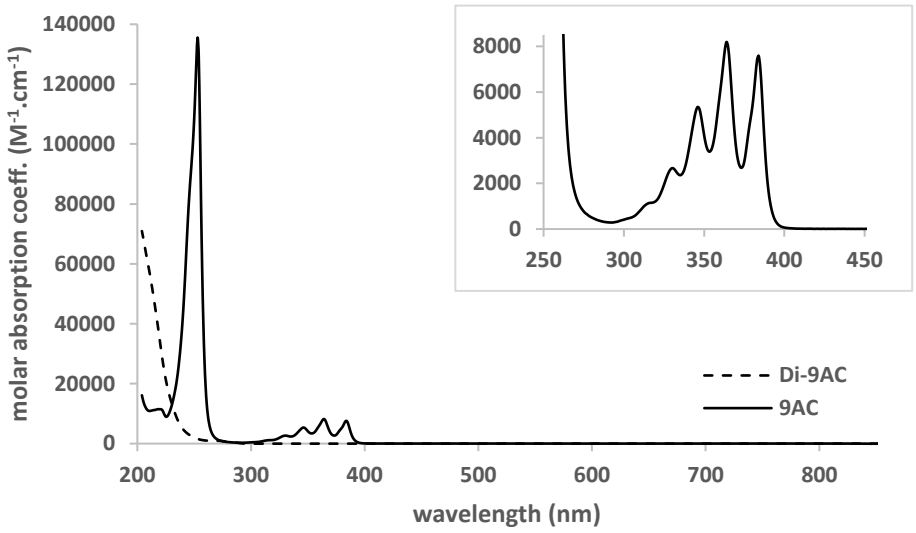

Figure S10: UV-vis spectra of Di-9AC and 9AC.

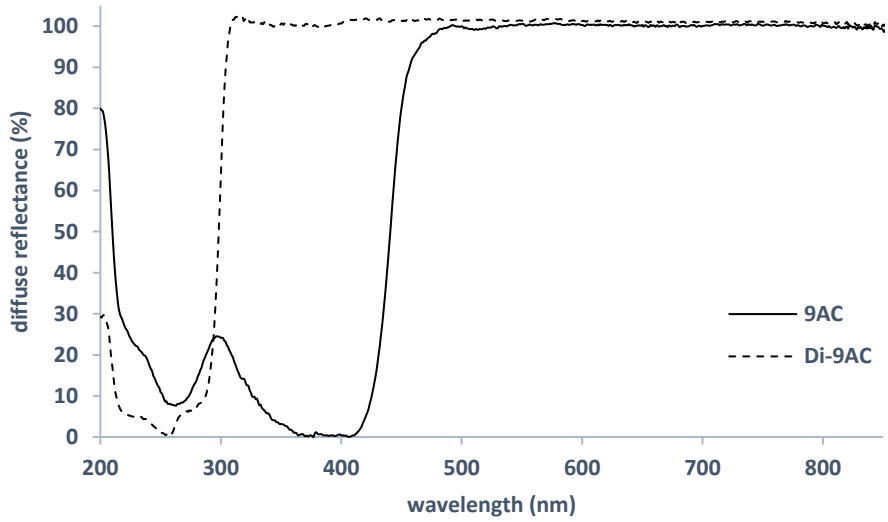

Figure S11: Diffuse reflectance spectra of Di-9AC and 9AC.

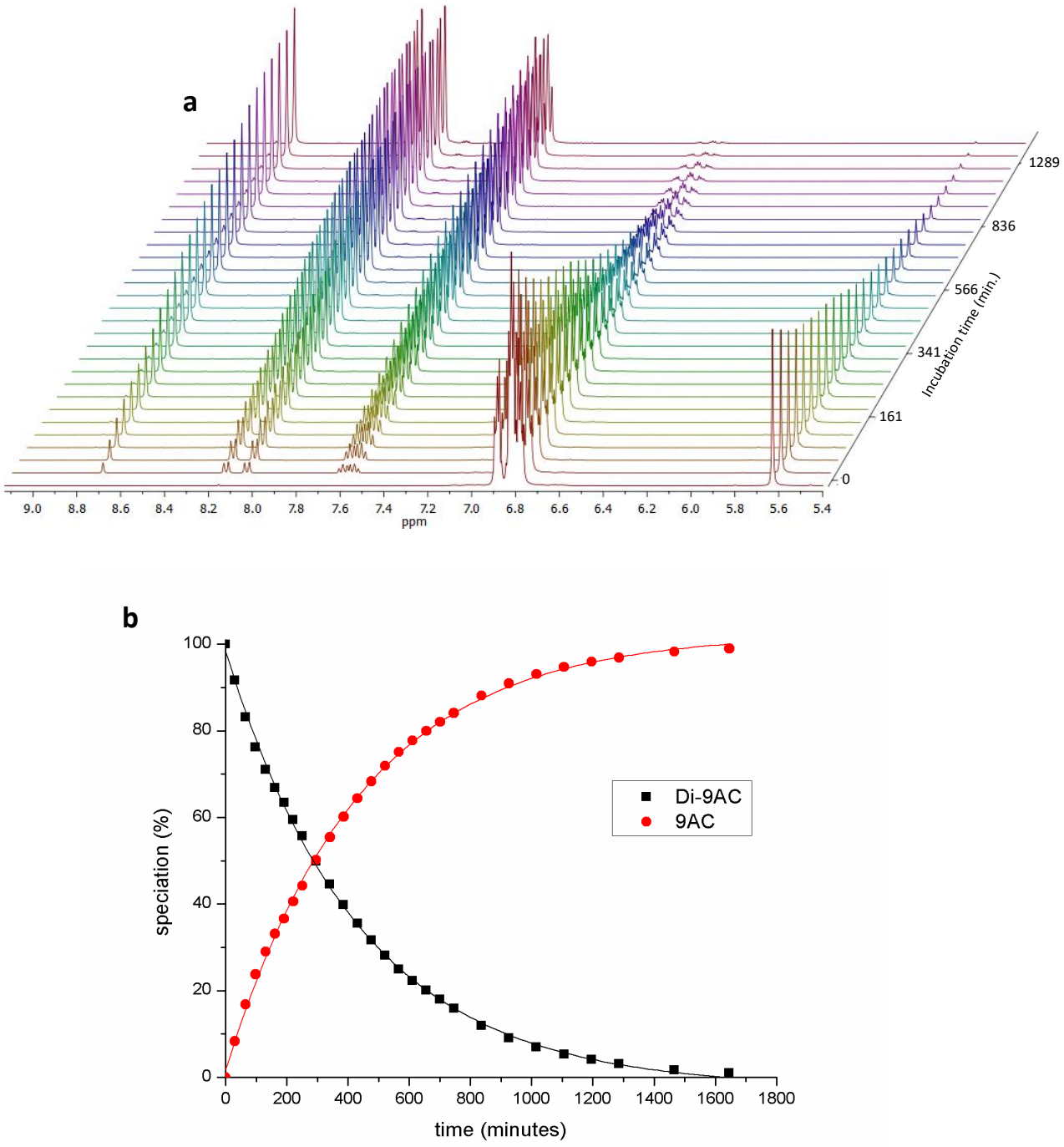

Figure S12: a, ^{1}H NMR spectra collected to monitor the thermocleavage at 130°C of Di-9AC followed over time (DMSO-d_6, 298 K). b, Speciation curves from the analysis of ^{1}H NMR data representing the quantification of Di-9AC (black) and 9AC (red) as function of time at 130°C.

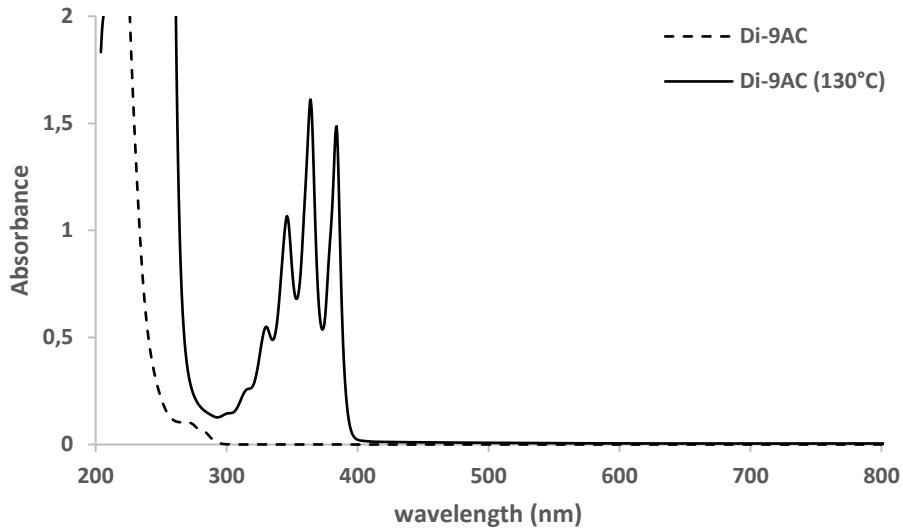

Figure S13: UV-vis absorption spectra showing the Di-9AC cleavage into 9AC (thermal treatment, 130°C, 48 hours).

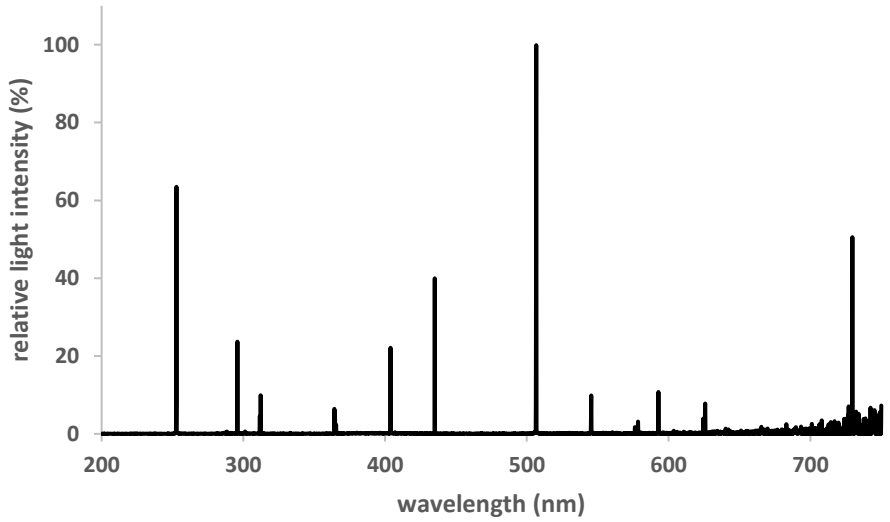

Figure S14: UV lamp spectrum used for photocleavage experiments (UV-Pen).

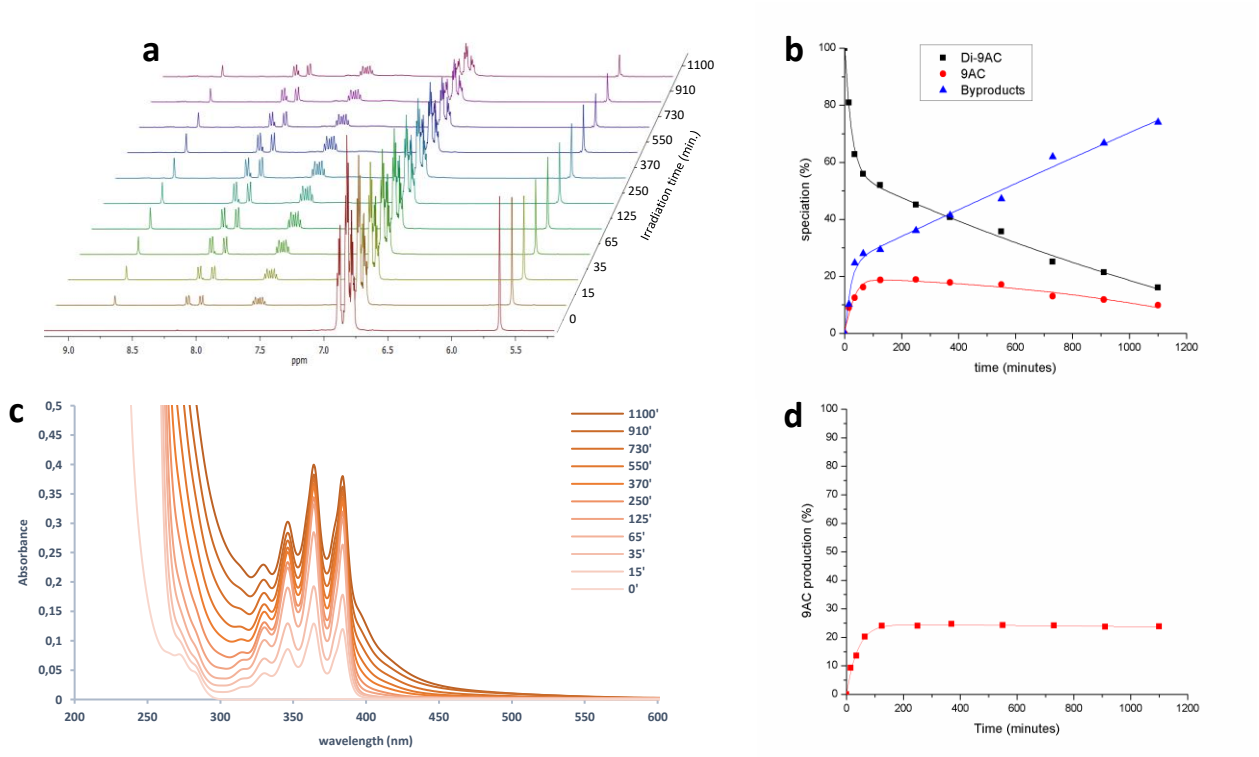

Figure S15: (a) ^{1}H NMR spectra of the Di-9AC collected after increasing irradiation times with the UV-Pen at 254 nm wavelength. (b) Quantification by ^{1}H NMR of the photocleavage of the Di-9AC into 9AC and byproducts obtained at different irradiation times at 254 nm. (c) UV-vis absorbance spectra showing the appearance over time of the 9AC upon the irradiation at 254 nm of the Di-9AC. (d) Quantification by UV-vis absorbance of the 9AC at different irradiation time at 254 nm.

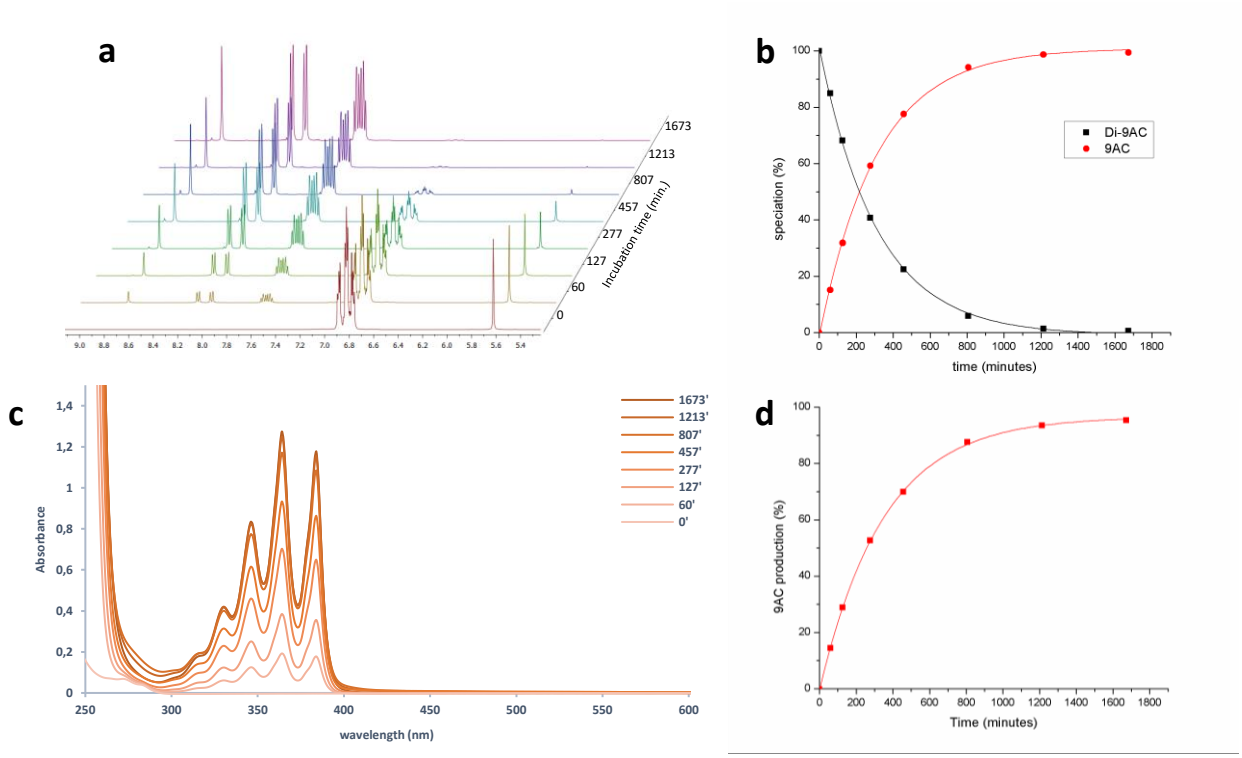

Figure S16: (a) ^{1}H NMR spectra of the Di-9AC collected after increasing incubation times at 130°C. (b) Quantification by ^{1}H NMR of the thermocleavage of the Di-9AC into 9AC and byproducts obtained at different incubation times at 130°C. (c) UV-vis absorbance spectra showing the appearance over time of the 9AC upon the incubation at 130°C of the Di-9AC. (d) Quantification by UV-vis absorbance of the 9AC at different incubation times at 130°C.

Table S4: Crystal data and structure refinement for CD-MOF-161

CCDC number	1835668
Empirical formula	$C_{70.77}H_{59.54}N_2O_{15}Yb_2$
Formula weight	1524.06
Temperature/K	180.15
Crystal system	triclinic
Space group	P-1
a/Å	16.6368(5)
b/Å	18.0871(6)
c/Å	19.3244(7)
α/°	84.612(3)
β/°	80.119(3)
γ/°	64.846(3)
Volume/Å^3	5184.0(3)
Z	2
ρ_{calc}g/cm^3	0.976
μ/mm^{-1}	3.669
F(000)	1516.0
Crystal size/mm^3	0.126 × 0.069 × 0.036
Radiation	CuKα (λ = 1.54184)
2Θ range for data collection/°	5.932 to 147.382
Index ranges	$-20 \leq h \leq 7$, $-22 \leq k \leq 21$, $-24 \leq l \leq 23$
Reflections collected	36773
Independent reflections	20325 [R_{int} = 0.0396, R_{sigma} = 0.0653]
Data/restraints/parameters	20325/170/897
Goodness-of-fit on F^2	0.965
Final R indexes [I>=2σ (I)]	R_1 = 0.0590, wR_2 = 0.1613
Final R indexes [all data]	R_1 = 0.0734, wR_2 = 0.1744
Largest diff. peak/hole / e Å^{-3}	3.21/-1.30

Figure S17: View of the asymmetric displacement ellipsoids are depicted at 50 percent probability level.

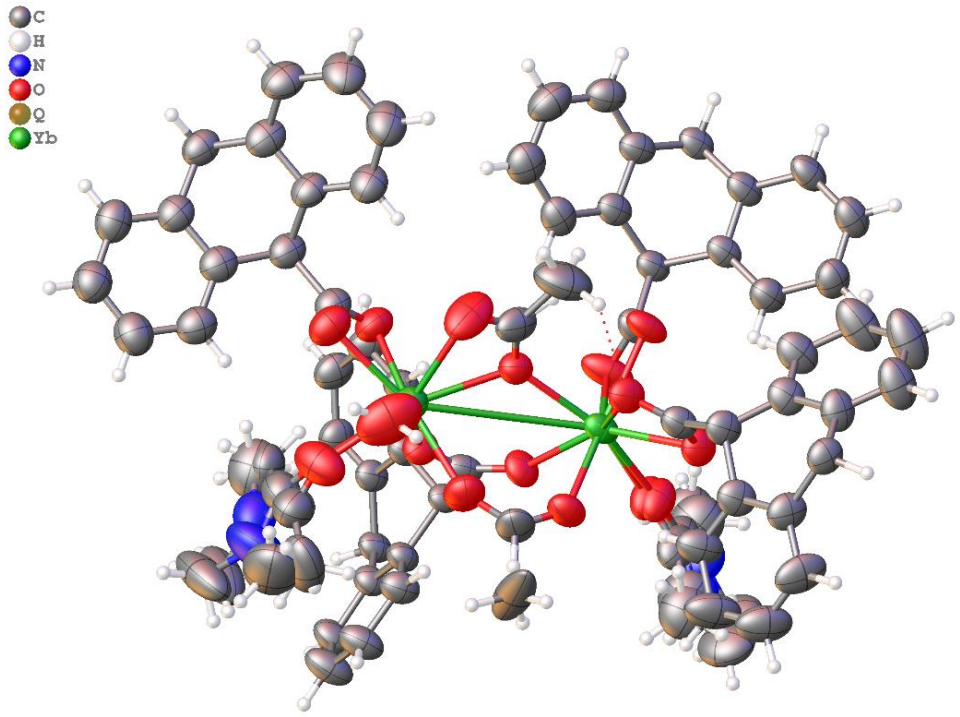

Table S5: Selected interatomic distances for CD-MOF-161

Atom	Atom	Length/Å	Atom	Atom	Length/Å
Yb1	Yb2	4.2584(5)	Yb2	O15	2.429(4)
Yb1	O15	2.306(4)	Yb2	O11	2.347(4)
Yb1	O4	2.341(3)	Yb2	O8	2.451(6)
Yb1	O3	2.408(4)	Yb2	O10	2.252(4)
Yb1	O2	2.349(3)	Yb2	O12	2.394(5)
Yb1	O6	2.242(3)	Yb2	O9	2.252(4)
Yb1	O5	2.263(4)	Yb2	O13	2.288(7)
Yb1	O1	2.388(4)	Yb2	O14B	2.249(14)
Yb1	O7B	2.305(10)	Yb2	O14A	2.255(10)
Yb1	O7A	2.211(8)	Yb2	O15	2.429(4)
Yb1	Yb2	4.2584(5)			

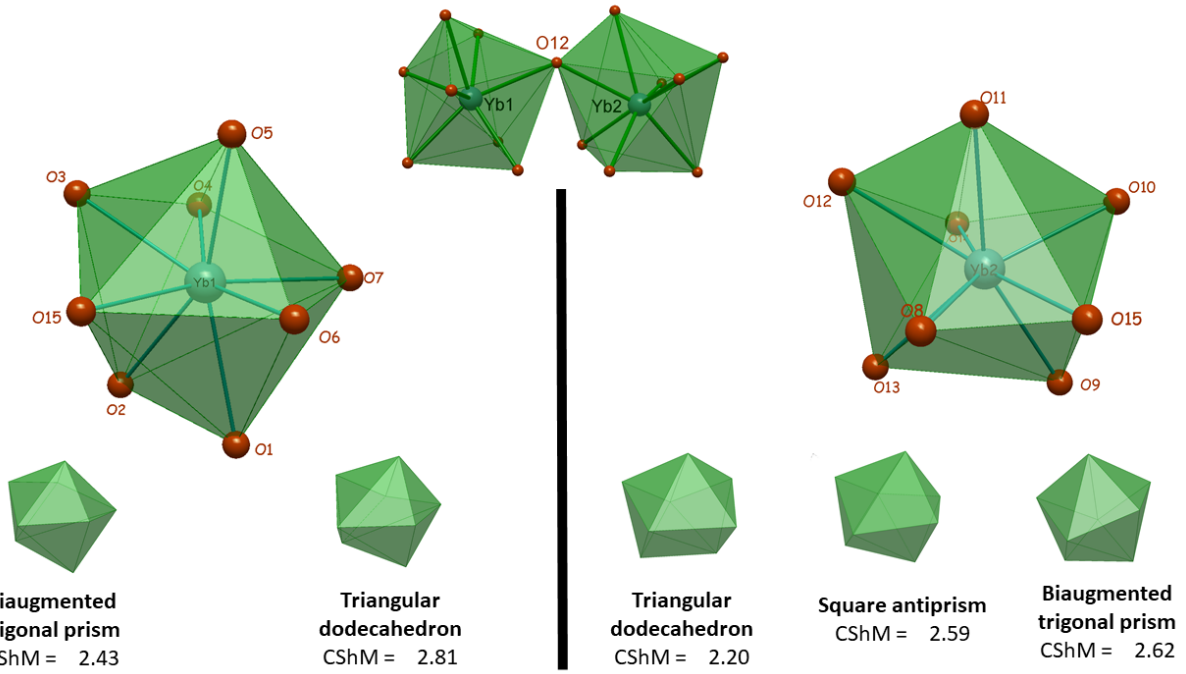

	Yb1	**Yb2**
Square antiprism	3.924	2.587
Triangular dodecahedron	2.805	2.203
Biaugmented trigonal prism J50	3.146	3.333
Biaugmented trigonal prism	2.432	2.618

Figure S18: Drawings of the shapes of each of the coordination polyhedron of the two ytterbium (Yb1 and Yb2) composing the dinuclear clusters in CD-MOF-161. The table below show results obtained with the SHAPE software used to calculate the continuous shape measure (CShM) values between these coordination polyhedra and some idealized ones.

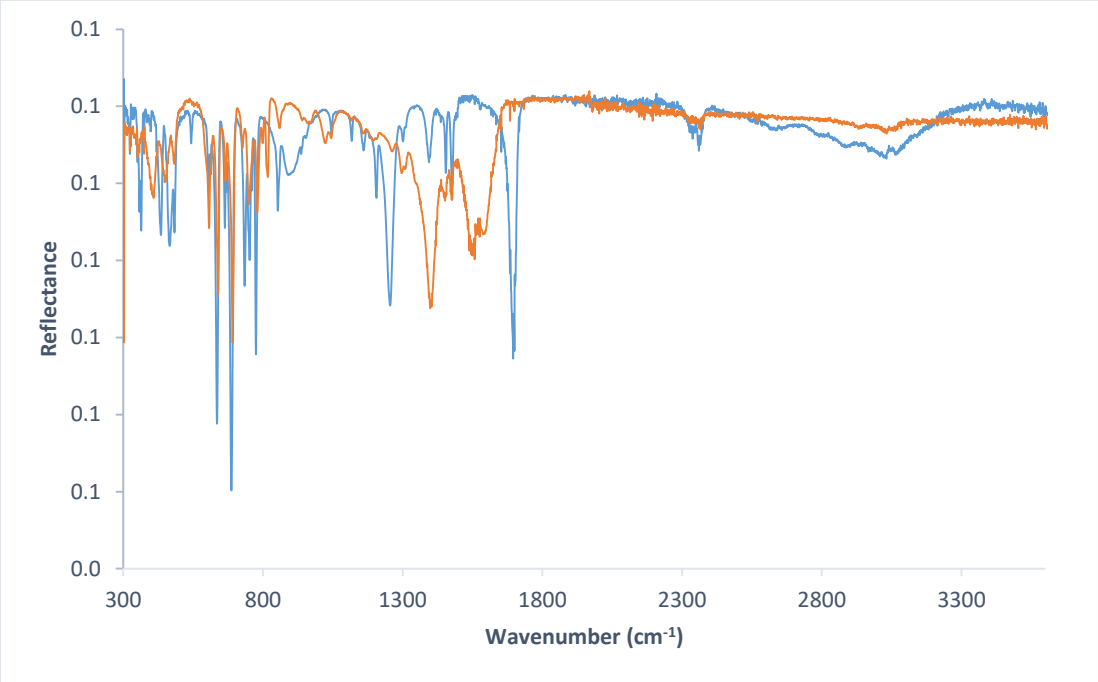

Figure S19: FTIR spectra of Di-9AC (blue) and CD-MOF-161 (orange).

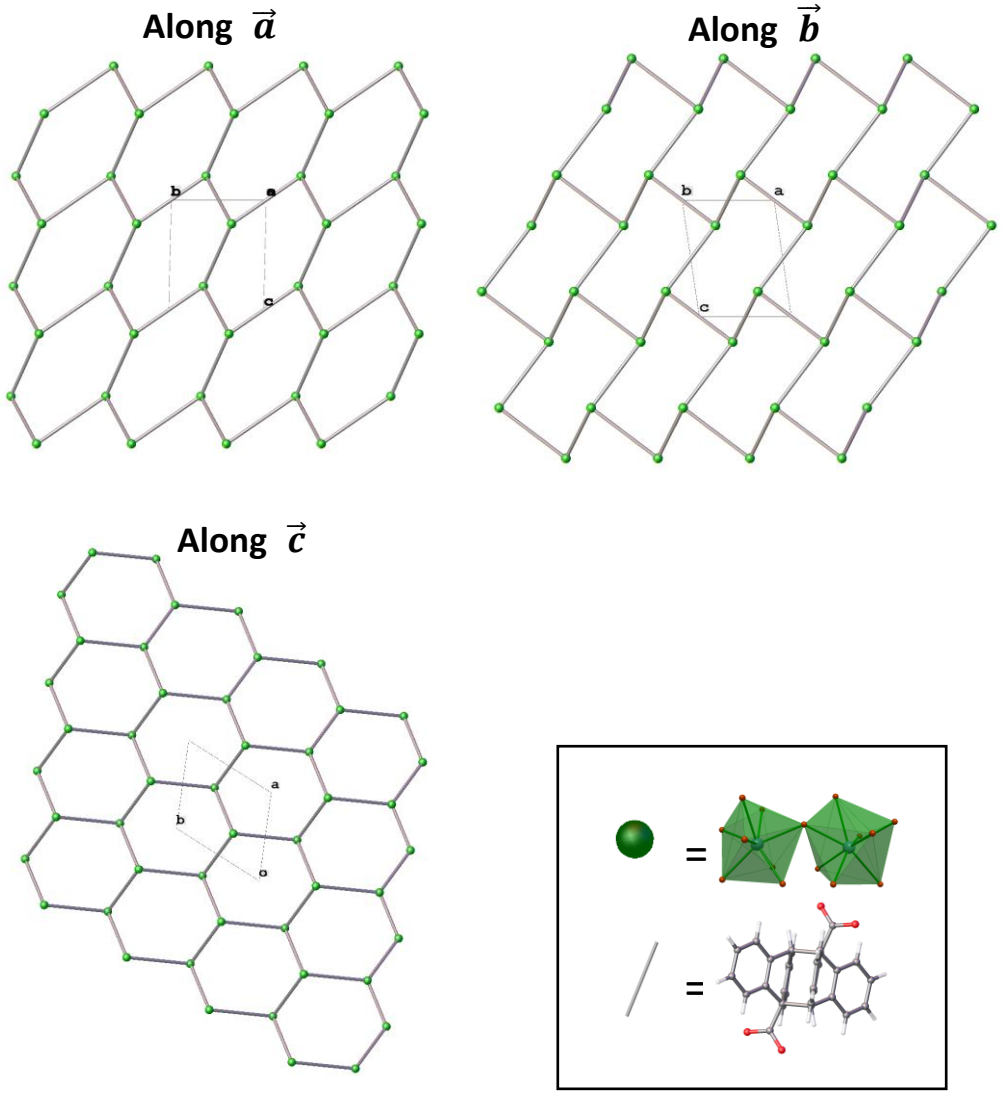

Figure S20: Topological view of CD-MOF-161 along the 3 axis, respectively a, b and c.

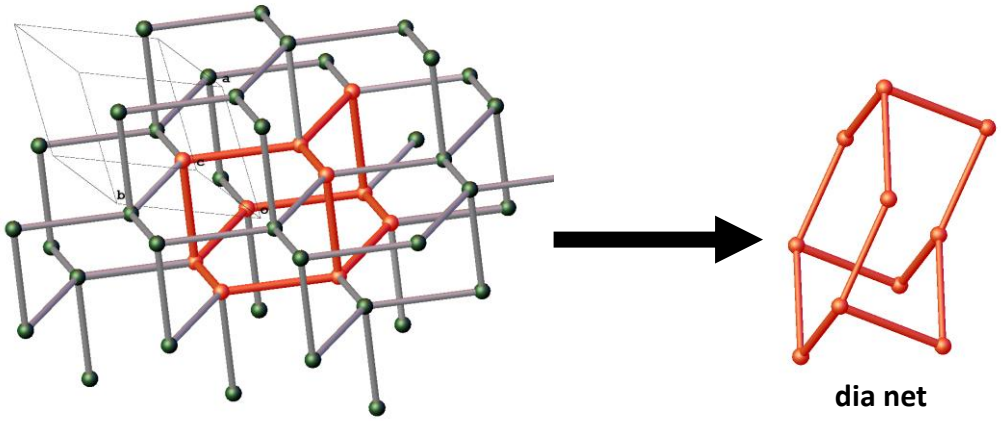

Figure S21: Topological analysis of CD-MOF-161 showing the typical pattern of the dia net (in red) into the crystal network.

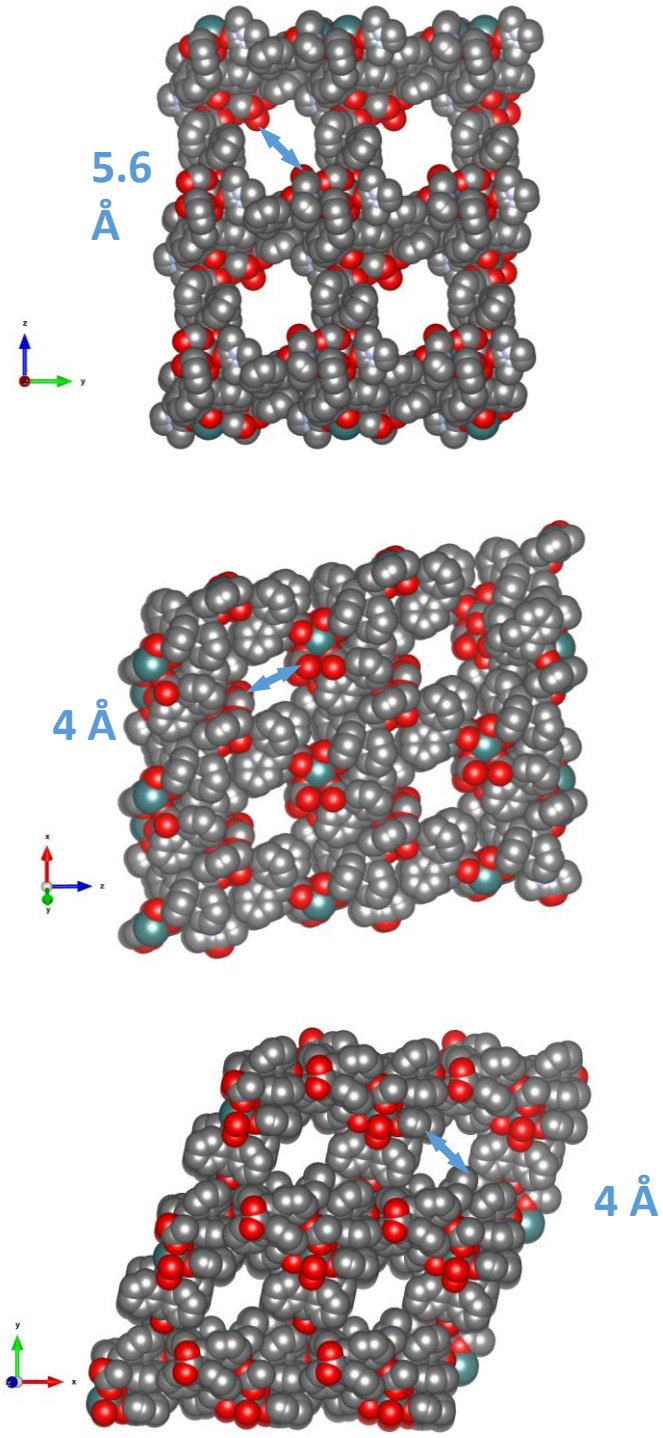

Figure S22: Interconnected mesoporous channels of CD-MOF-161 in different directions. Crystallographic a direction (top), Crystallographic b direction (0, -1, 1) (middle), Crystallographic c direction (0, 1, -1) (bottom).

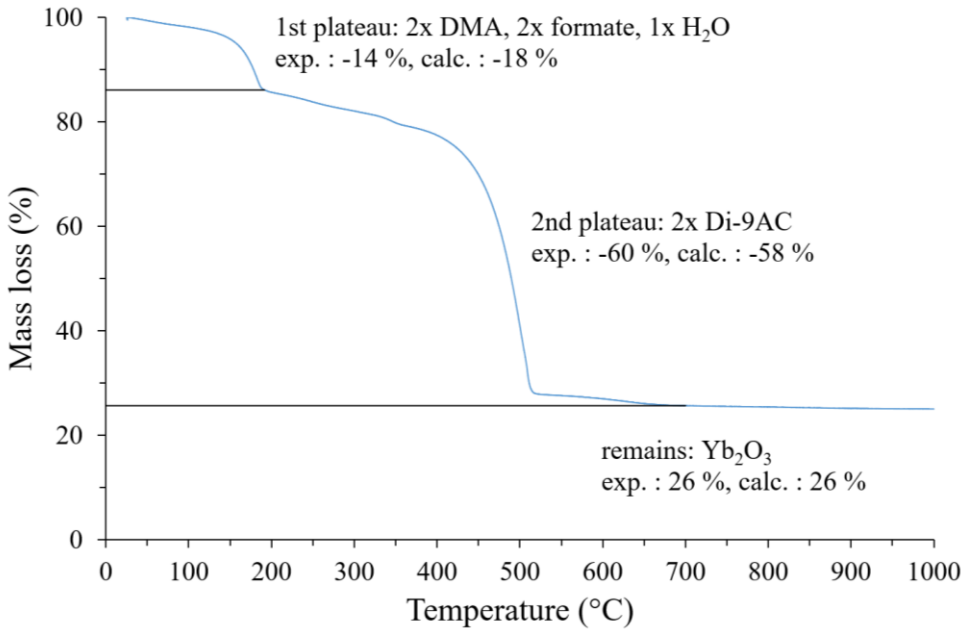

Figure S23: TGA profile of CD-MOF-161.

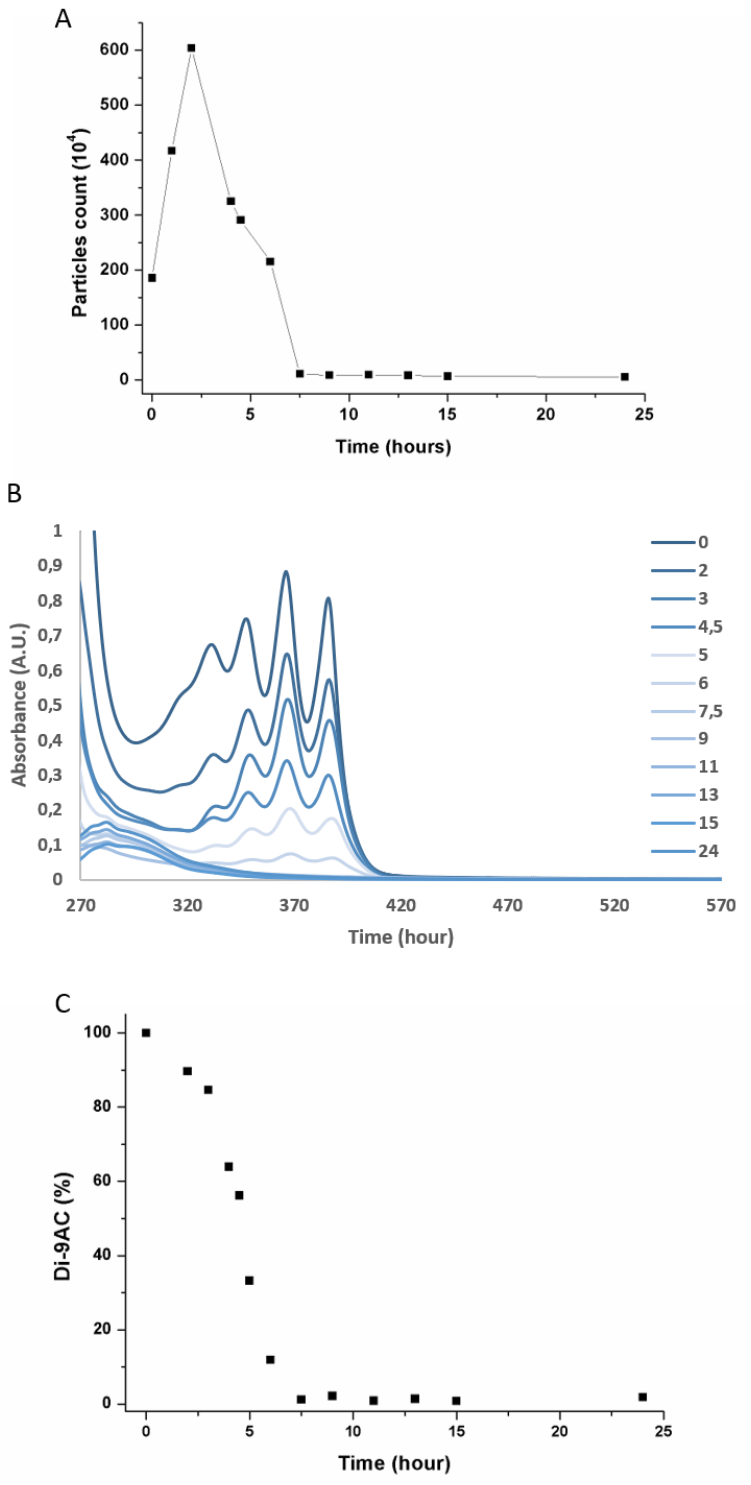

Figure S24: (A) Quantification of the number of CD-MOF-161 particles along the irradiation time with the 254 nm UV-Pen obtained from the analysis of brightfield microcopy images. (B) UV-vis absorbance spectra of 9AC resulting from the thermocleavage of remaining CD-MOF-161 collected after various time

of irradiation with the UV-Pen at 254 nm wavelength. (C) Quantification by UV-vis absorbance spectroscopy of the ligand of the remaining CD-MOF-161 after the different irradiation times with the 254 nm wavelength.

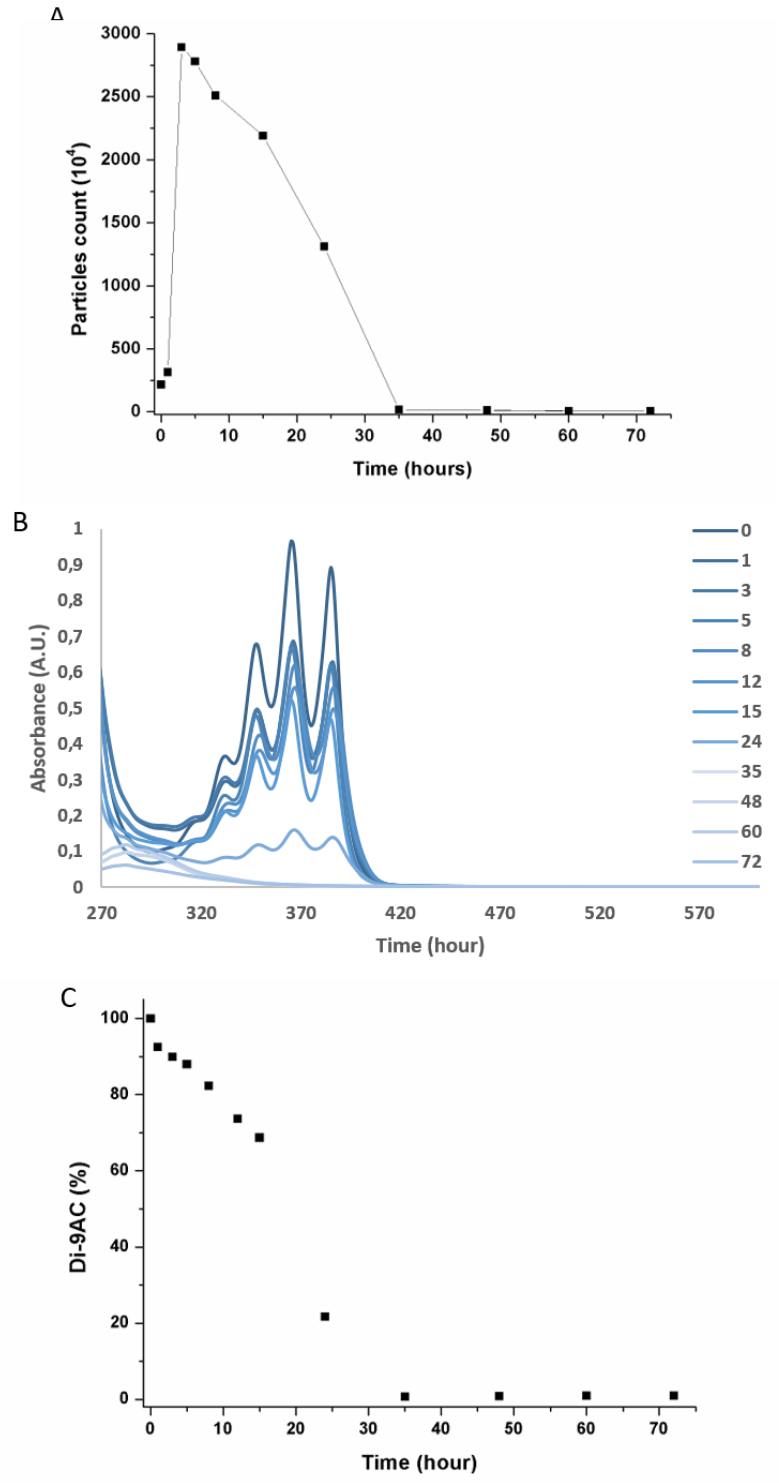

Figure S25: (A) Quantification of the number of CD-MOF-161 particles along the incubation time at 160°C obtained from the analysis of brightfield microcopy images. (B) UV-vis absorbance spectra of 9AC resulting from the thermocleavage of remaining CD-MOF-161 collected after various time of incubation

at 160°C. (C) Quantification by UV-vis absorbance spectroscopy of the ligand of the remaining CD-MOF-161 after the incubation times at 160°C.

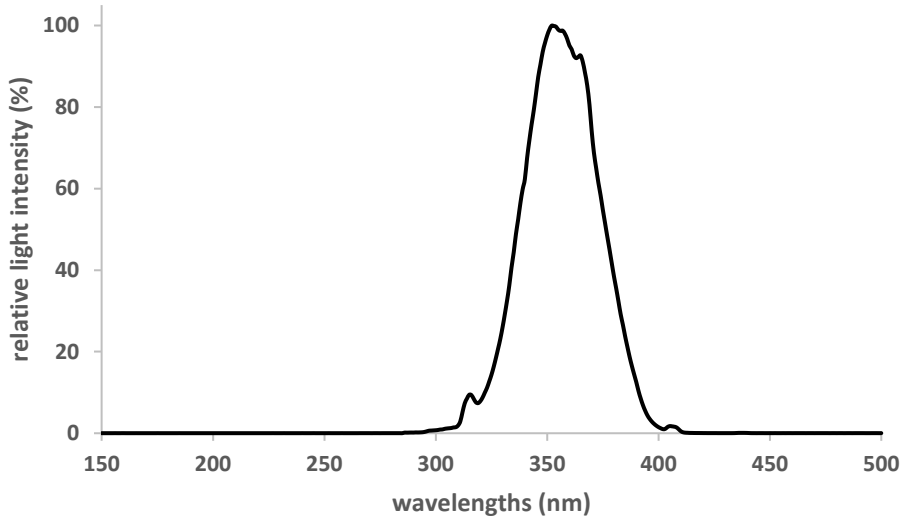

Figure S26: Spectrum of the UV-lamp used for the photodimerization experiments (Vilber-Lourmat).

1) Irradiation of CD-MOF-161 suspended in DMA (3 mL in quartz cuvette)
2) Transfer of the suspension into centrifuge tubes (15 mL tubes)
3) Pellet of the remaining CD-MOF-161 obtained by centrifugation, 3500 RCF, 10 min., RT
4) Removal of the supernatant
5) Washing of the pellet of remaining materials 3 times with fresh DMA

- resuspension of the pellet in 10 mL of fresh DMA
- centrifugation, 3500 RCF, 10 min., RT
- removal of the supernatant

3x

6) Addition of 3 mL of fresh DMA
7) Heating at 160°C, 48 h
8) UV-vis absorbance spectroscopy

Figure S27: Description of the sample processing prior absorbance spectroscopy measurements.

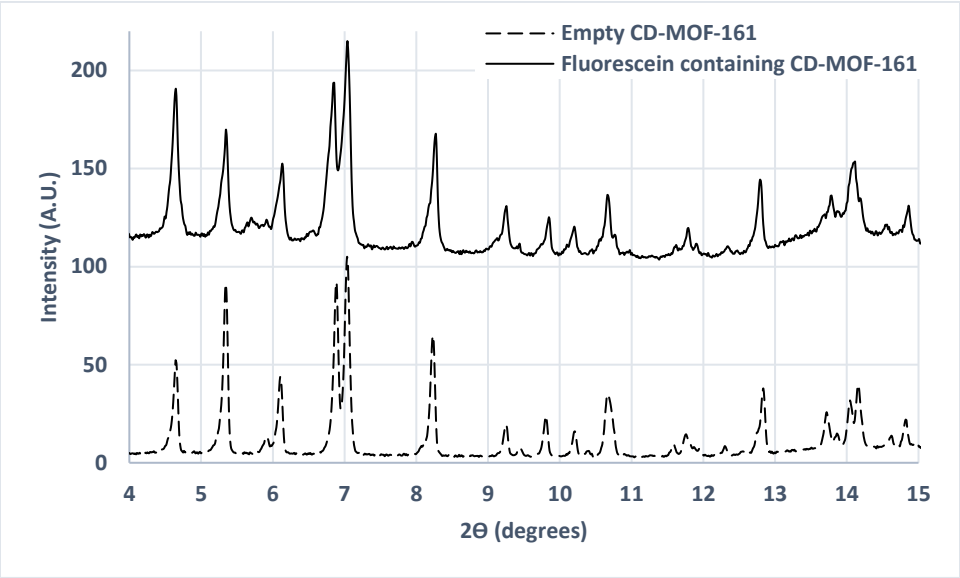

Figure S28: Comparison of the experimental powder diffraction patterns obtained from the empty CD-MOF-161 (dashed line) and the fluorescein containing CD-MOF-161 (continuous line).

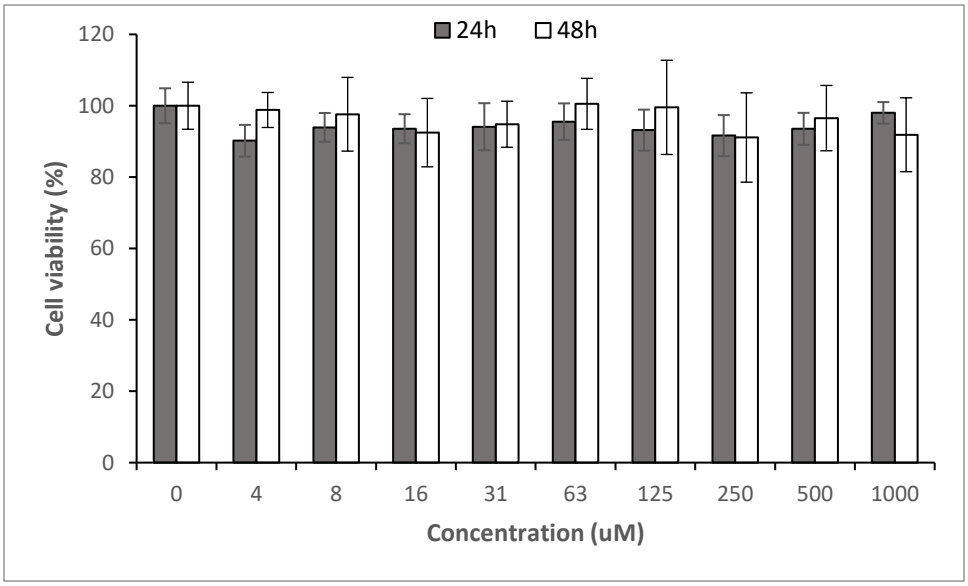

Figure S29: Cell cytotoxicity experiment performed on HeLa cells. Various amounts of $Yb(OAc)_3$ diluted in complete cell culture medium were incubated during 24 h (grey) and 48 h (white) with cells. Data are normalized on untreated cells considered as 100% of viability. Error bars represent the standard deviation.

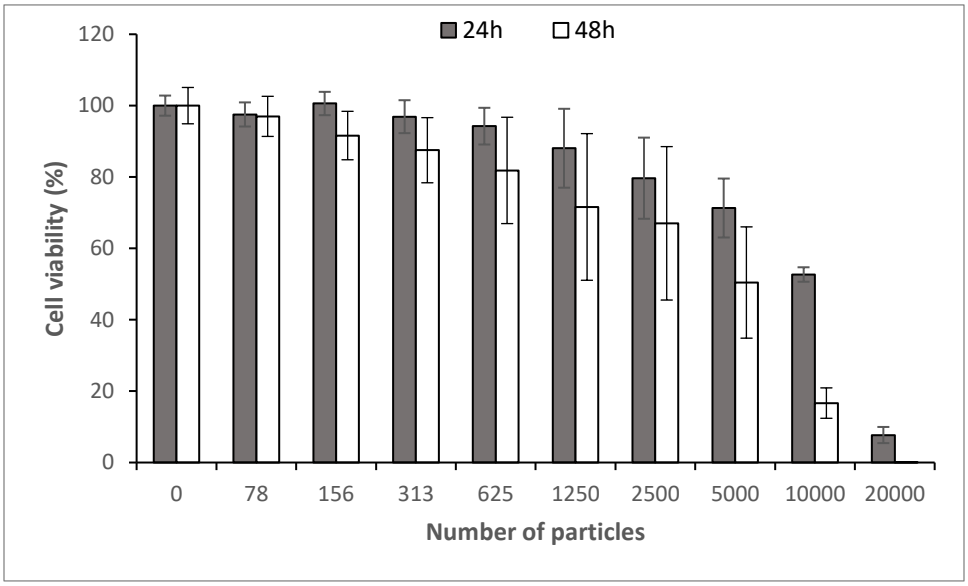

Figure S30 Cell cytotoxicity experiment performed on HeLa cells. Various amounts of CD-MOF-161 particles, collected directly after synthesis, were diluted in complete cell culture medium and incubated during 24 h (grey) and 48 h (white) with cells. Data are normalized on untreated cells considered as 100% of viability. Error bars represent the standard deviation.

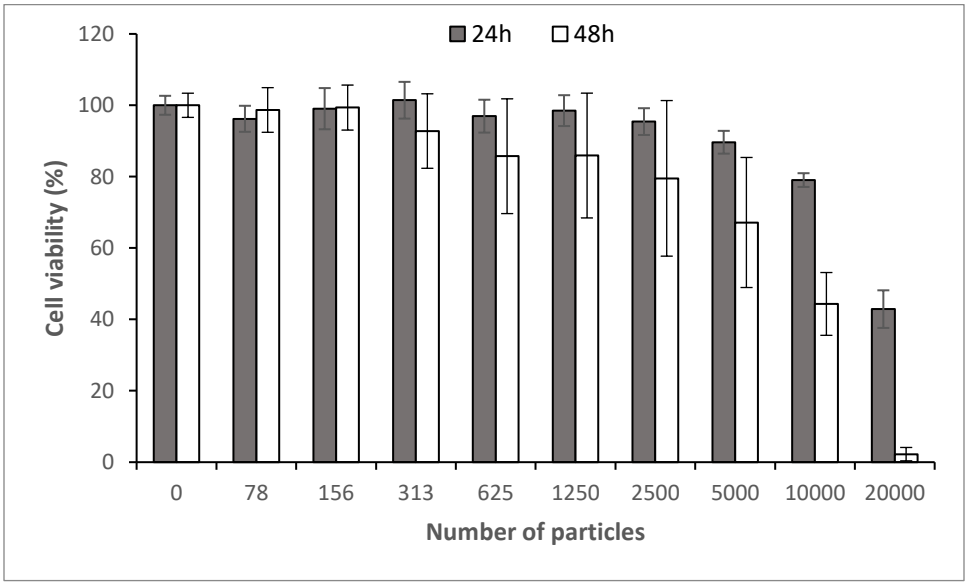

Figure S31: Cell cytotoxicity experiment performed on HeLa cells. Various amounts of CD-MOF-161 particles, left overnight in 15 mL of water for washing purpose, were diluted in complete cell culture medium and incubated during 24 h (grey) and 48 h (white) with cells. Data are normalized on untreated cells considered as 100% of viability. Error bars represent the standard deviation.